Cationic Basic Yellow 2 (BY2) adsorption onto manure ash: surface properties and adsorption mechanism

A. Öztürk, E. Malkoc*

Department of Environmental Engineering, Ataturk University, Erzurum, Turkey
Tel. +904422314603; Fax: +904422360957; email: emalkoc@atauni.edu.tr

ABSTRACT

Adsorption of Basic Yellow 2 (BY2) onto manure ash, a waste substance, was studied in batch and fixed-bed studies. In both systems, experiments were conducted by using the UV–visible spectroscopy and by examining the effect of different parameters. In order to obtain the adsorption mechanism of manure ash, its microstructure information must be studied. Surface area, particle size distribution (PSD), and structure of adsorbent were studied with Fourier transform infrared spectroscopy, transmission electron microscopy, and PSD. The surface measurement such as specific surface area and pore volume was measured and calculated using BET method. Nitrogen sorption measurements were employed to investigate the variation in surface and pores properties before and after dye adsorption. The experimental isotherm data were analyzed using Langmuir, Freundlich, Dubinin –Radushkevich (D–R), Temkin, Harkins–Jura, and Frumkin isotherm equations, but high correlation coefficients (R^2) confirmed the validity of Langmuir isotherm, with monolayer adsorption capacity (Q_0) equal to 1,666.7 mg/g at 45°C. A full thermodynamic evaluation was carried out, calculating the parameters of enthalpy, free energy, and entropy ($\Delta H°$, $\Delta G°$, and $\Delta S°$). The thermodynamics of BY2 onto manure ash system indicates spontaneous and endothermic nature of the process. The kinetic models: Lagergren's pseudo-first order, pseudo-second order, intra-particle diffusion, liquid-film diffusion, Bangham and Avrami kinetic models were applied to the experimental data. It was observed that pseudo-second-order kinetic model described the adsorption process better than any other kinetic models. The Adams–Bohart, Thomas, and Yoon–Nelson models were applied to the adsorption under varying experimental conditions to predict the breakthrough curves and to evaluate the model parameters of the fixed-bed column that are useful for process design.

Keywords: BET; PSD; TEM; Adsorption; Fixed-bed column; Dye; Adsorption kinetic

1. Introduction

The global problem of clean water shortage has been exacerbated by its pollution caused through discharge of untreated industrial effluents. The problem is further aggravated in developing countries owing to uncontrolled population growth, and the use of outdated practices and technologies that consume large volumes of water in agricultural and industrial operations [1]. Dye contamination in aqueous wastewater from industries is a serious problem because dyes are not biodegradable and tend to suppress

*Corresponding author.

photosynthetic activity in aquatic habitats by preventing the sunlight penetration [2]. Therefore, their removal from textile effluents has been the target of great attention in the last few years.

Cationic dyes are synthetic pigments, commonly known as basic dyes and are widely used in textile industry. Basic dyes are used in several processes such as acrylic, nylon, silk, and wool dyeing [3]. Basic Yellow 2 (BY2), a yellow dye, (4,4-dimethylaminobenzophenonimide) and its hydrochloride salt are used in the coloring of paper, textiles, and leather [4]. The efficiency of dyeing process is often poor, resulting in an escape of a large quantity of dyes through wastewater [3]. The heavy metals in the basic dyes could accumulate in the environment and may cause serious long-term effects to ecosystem. In addition, this group of dyes includes a broad spectrum of different chemical structures, primarily based on the substituted aromatic groups which are resistant to both chemical and biological breakdowns, which may otherwise produce small amount of toxic and carcinogenic products [3,5].

Several conventional wastewater treatment technologies have been applied for dye removal, including physical, chemical, and biological processing [6]. The treatment method selected will depend primarily on the pollutant concentration, the effluent flow, and the discharge body [7]. These processes are costly and cannot effectively be used to treat the wide range of dye wastewater [3,8].

Adsorption has been proven to be an effective process for dye removal due to its low cost, high adsorption capacity, and environmental friendliness [9]. Generally, adsorbents provide a large surface area, which interact with contaminant molecules and can adsorb them by physical or chemical interaction. Capital cost and regeneration property of adsorbent material affect the industrial application of adsorption process for the removal of pollutants. As an example, activated carbon has proven to be one of the most effective and reliable adsorbent for decolorization of wastewater, but it is still expensive and cannot be easily regenerated [10]. Consequently, low-cost potential adsorbents are sought in dye removal, such as chitosan [11], activated carbon prepared from paper mill sewage sludge [12], pine sawdust [13], kaolin [14], wheat bran [15], poplar sawdust [16], boron industry waste [17], grapefruit peel [1], de-oiled soya [18], peat [19], and natural phosphate [20].

The aim of the present work is to explore the possibility of manure ash for the adsorptive removal of BY2 from wastewater using batch and fixed-bed column. In batch studies, the dynamic behavior of the adsorption was investigated on the effect of temperature at different BY2 concentrations. Different adsorption kinetics and isotherm models were applied to the experimental data. The thermodynamic parameters were also evaluated from the adsorption measurements. The important design parameters such as flow rate, bed depth, and initial concentration of BY2 have been investigated and breakthrough curves for the adsorption of dye were analyzed using Adams–Bohart model, Yoon–Nelson, and Thomas models.

2. Experimental

2.1. Adsorbent and characterization of adsorbent

In this study, as adsorbent ash of manure used as fuel especially in rural areas was used. Bovine animal wastes (manure) were dried naturally and as an alternative to wood and coal is used for heating. Ash obtained from combustion is used as adsorbent. It is a completely natural adsorbent and a waste substance. The physical characteristics of the manure ash are presented in Table 1.

Fourier transform infrared (FTIR) spectra were measured using Perkin–Elmer Spectrum One model FTIR spectrometer. The particle size distributions (PSD) of the solid samples were determined using a Malvern Mastersizer 2000 particle analyzer.
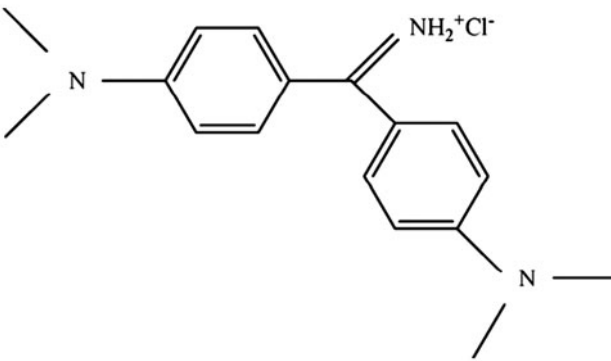
The specific surface area and average pore size of the manure ash samples were analyzed using, the BET and BJH methods, respectively. The determinations of the surface area and pore size were based on isotherms of adsorption and desorption of nitrogen at $77 \pm 0.5\,K$ using a Gemini V2.00 Surface Analyser (Micromeritics, USA). Before measurements, moisture and gases such as nitrogen and oxygen that were adsorbed on the solid surface or held in the open pores were removed under reduced pressure at 423 K for 7 h.

The evolution of the morphology and particle size of the nano-mixed oxide powders was examined by transmission electron microscopy (TEM) using a JEM-100S electron microscope (Jeol, JEM-100SX Electron Microscope, Tokyo, Japan).

Table 1
Physical properties of manure ash used in the experiments

Physical characteristic	Units
Bulk density (g/cm^3)	0.256
BET surface area (m^2/g)	15.6593
Particle size (mm)	0.10–0.15

Table 2
Physicochemical properties of BY2 dye

Molecular structure [21]	

Color index name	Basic Yellow 2 (BY2)
Commercial name	Auramine-O
Molecular formula	$C_{17}H_{21}N_3 \cdot HCl$
Molecular weight (g mol^{-1})	303.83
λ_{max} (nm)	432

2.2. Adsorbate

The BY2, was obtained from Aldrich company and used without further purification. The dye solutions used in the experiments (1000 mg/L) were prepared by dissolving the required amount of dye in distilled water. The physicochemical properties of BY2 are shown in Table 2.

2.3. Batch and fixed-bed adsorption experiments

Experiments were conducted in 250 mL -Erlenmeyer flasks containing known BY2 synthetic solutions. Flasks were agitated on a shaker at 240 rpm constant shaking rate for 150 min to ensure equilibrium was reached and filtered through (Schleicher & Schull 589). Samples of volume 5 mL were taken after mixing the adsorbent and BY2 solution bearing solution and at predetermined time intervals (1–150 min) for the determination of residual BY2 concentration. pH was adjusted by the addition of dilute aqueous solutions of HCl or NaOH (0.01 M). The initial and equilibrium BY2 concentrations were determined by absorbance measurement using a double beam UV–vis spectrophotometer at 432 nm. The kinetics of adsorption was determined by analyzing adsorptive uptake of the dye from the aqueous solution at different time intervals. For adsorption isotherms, dye solutions of different concentrations were agitated with the known amount of adsorbent till the equilibrium was achieved. The residual dye concentration (C_e) of the solution was then determined. The percentage removal of BY2 and equilibrium adsorption uptake, q_e (mg/g), was calculated using the following Eqs. (1) and (2) [21]:

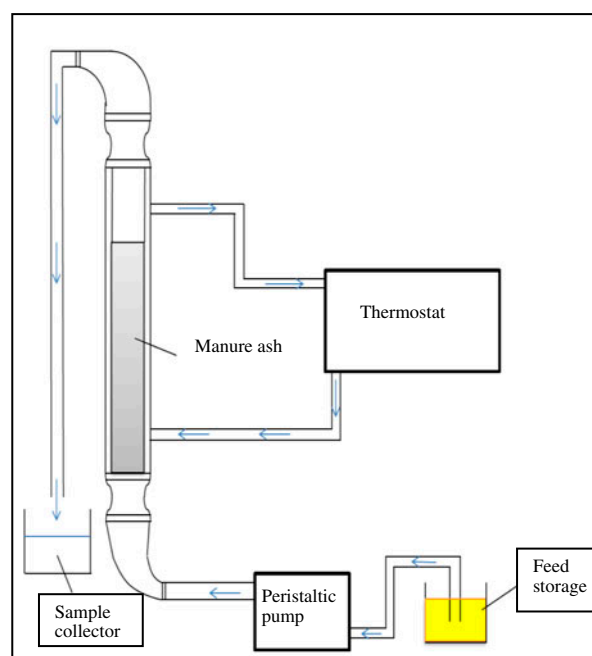$$\% \text{ Removal} = \frac{C_0 - C_e}{C_e} \tag{1}$$

Fig. 1. Experimental setup for fixed bed operation.

Amount adsorbed $(q_e) = \dfrac{C_0 - C_e}{m} \left(\dfrac{mg\,BY2}{g\,adsorbent} \right)$ (2)

where C_0, C_e, and m is the initial BY2 concentration, equilibrium BY2 concentration (mg/L), and adsorbent mass (g/L), respectively.

A schematic diagram for the pilot plant fixed-bed column is shown in Fig. 1. The fixed-bed columns were made of Perspex tubes 2.0 cm internal diameter and 30 cm in height. The bed length used in the experiments was 4.5 cm. In a typical experiment, the known dye concentrations was pumped at a fixed flow rate to filled the bed depth. The pH of the solutions was maintained constant at 7.0. The temperature of stream feeding solution and of the column was controlled at 25°C through a thermostatic bath.

The time for breakthrough appearance and the shape of the breakthrough curve are very important characteristics for determining the operation and the dynamic response of an adsorption column. The breakthrough curves show the loading behavior of dye to be removed from solution in a fixed bed and is usually expressed in terms of adsorbed dye concentration (Cad = inlet dye concentration, (C_0) – outlet dye concentration, (C_t)) or normalized concentration defined as the ratio of effluent dye concentration to inlet dye concentration (C_t/C_0) as a function of time or volume of effluent (V_{eff}) for a given bed depth (in Eq. (3)) [22,23].

$V_{eff} = Qt$ (3)

where t and Q are the total flow time (min) and volumetric flow rate (mL/min). The area under the breakthrough curve (A) obtained by integrating the adsorbed concentration (Cad; mg/L) vs. t (min) plot can be used to find the total adsorbed dye quantity (maximum column capacity). Total adsorbed dye quantity (q_{total}; mg) in the column for a given feed dye concentration and flow rate is calculated from the following Eq. (4) [24]:

$q_{total} = \dfrac{QA}{1000} = \dfrac{QA}{1000} \displaystyle\int_{t=0}^{t=total} C_{ad}\,dt$ (4)

where t_{total}, Q and A are the total flow time (min), flow rate (mL/min), and the area under the breakthrough curve, respectively.

Equilibrium dye uptake (q_{eq}) (or maximum capacity of the column) in the column is defined by Eq. (5) as the total amount of dye sorbed (q_{total}) per g of sorbent (X) at the end of total flow time [22]:

$q_{eq} = \dfrac{q_{total}}{X}$ (5)

3. Results and discussion

3.1. Characterization of manure ash

3.1.1. FTIR analysis

The FTIR spectrum is carried out as a qualitative analysis to determine the main functional groups that are involved in the dye adsorption process. The FTIR spectrum of the manure ash is shown in Fig. 2(a) and (b). The FTIR spectra were recorded from 4000 to 450 cm^{-1} in transmission mode. From this figure, it is possible to verify the complex nature of this adsorbent.

Investigations of spectrum of manure ash, carboxyl groups are observed as band at 1665–1760 cm^{-1} (1668 cm^{-1}), whereas the band at ~1600 cm^{-1} is attributed to the presence of epoxy groups and to C=C stretching mode of the sp^2 carbon skeletal network [25]. Also, carboxylic group peak after BY2 adsorption
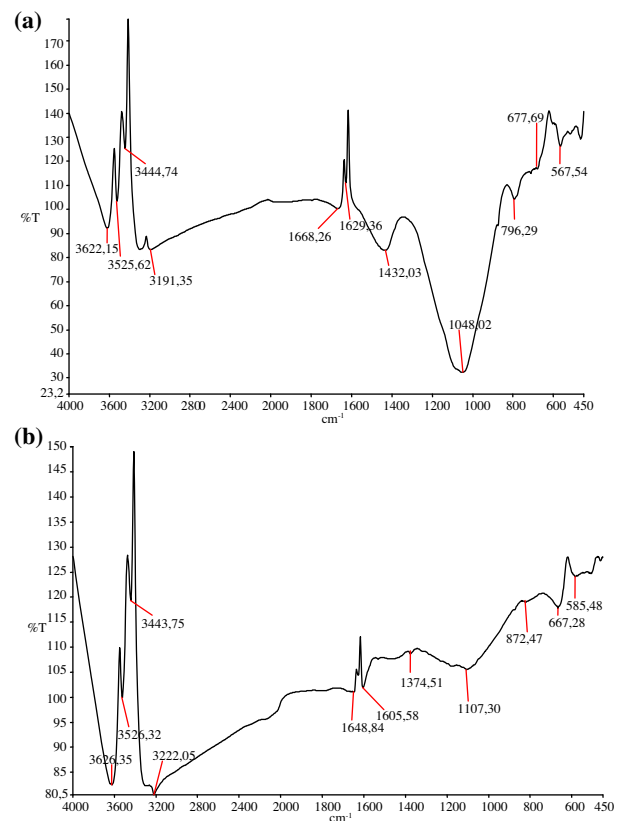

Fig. 2. FTIR (a) raw manure ash (b) manure ash after BY2 adsorption.

was observed at 1648. That means amount of carboxylic groups were changed because of dye adsorption [26]. The broad band between 2200 and 3800 cm^{-1} (3622, 3525, 3444, 3191 cm^{-1} before BY2 adsorption and 3626, 3526, 3443, 3222 cm^{-1} after BY2 adsorption) correspond to O–H groups [25] (alcohols, phenols, and carboxylic acids), which are either attached to carbons or represent adsorbed water. The O–H stretching vibrations occur within a broad range of frequencies indicating the presence of "free" hydroxyl groups and bonded O–H bands of carboxylic acids [27].

Asymmetric stretching vibration of ionic carboxylic groups appears at 1629 cm^{-1} [27]. FTIR spectrum of manure ash showed the intense bands at 1432 cm^{-1} which shifted to 1374 cm^{-1} that indicated the responsibility of alkane group for the adsorption process [28]. A remarkable broad band in the region 1000–1300 cm^{-1} (1048 and 1107 cm^{-1} before and after adsorption, respectively) is detected, which is associated with the stretching mode of vibrations O–H alcohols (primary and secondary) and −SO$_3$ stretching of aliphatic ethers and C–O stretching of COOH [26]. The sharp bands observed between 700 and 900 cm^{-1} could be assigned to S–OR esters. This band is observed to shift to 872 from 796 cm^{-1} in adsorption process [26]. The intense peaks at ~677 and 667 cm^{-1} indicate an N–H stretch (primary and secondary amines) [29]. The absorption peak around 567 cm^{-1} is attributed to the stretching vibration of BY2, the absorption peaks shift to 585 cm^{-1} after dye adsorption, which indicated that dye ions participated in the adsorption process.

As a results, the spectral analysis before and after BY2 adsorption indicated that especially the bonded O–H groups, carboxyl groups, alkane groups, S–OR esters, N–H stretching, −SO$_3$ stretching, C–O stretching, and −CN stretching were especially involved in BY2 adsorption. The adsorption of dye onto the manure ash may likely be due to the electrostatic attraction between these groups and the dye molecules.

3.1.2. PSD

The PSD of pure manure ash and samples taken at regular intervals during BY2 adsorption process were measured using a laser diffraction technique with a Malvern Mastersizer 2000. In adsorption experiments carried out, the conditions adsorbent concentration: 0.1 g/L, agitation speed: 240 rpm, pH 7.0, and BY2 concentration: 100 mg/L, samples were taken at 1, 10, 30, 60, and 150 min. Changes in PSD during the

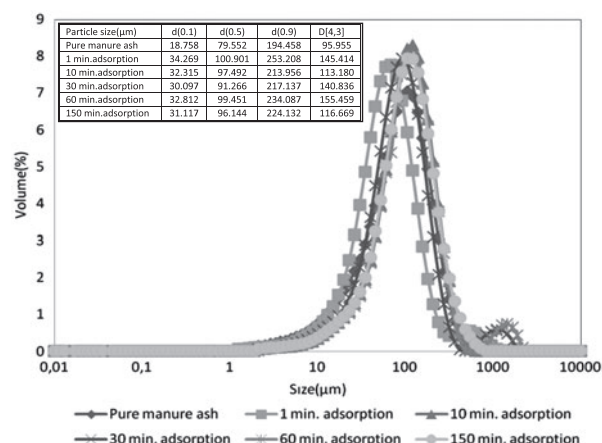| Particle size(µm)	d(0.1)	d(0.5)	d(0.9)	D[4,3]
Pure manure ash	18.758	79.552	194.458	95.955
1 min.adsorption	34.269	100.901	253.208	145.414
10 min.adsorption	32.315	97.492	213.956	113.180
30 min.adsorption	30.097	91.266	217.137	140.836
60 min.adsorption	32.812	99.451	234.087	155.459
150 min.adsorption	31.117	96.144	224.132	116.669

Fig. 3. PSD of manure ash during the adsorption process.

adsorption process are investigated. The results are presented in Fig. 3.

As seen in Fig. 3, we have found that the PSD at 1 min are nearly the same with at 10, 30, 60, and 150 min. The size distributions of particle, before and after adsorption, were in the range between 3 and 1096 µm. Also, in Fig. 3, it can be seen that all the adsorbent follow good logarithmic distribution and adsorbents before and after BY2 adsorption are similar to each other. Fifty percent of the pure manure ash was less than 79.552 µm in size, whereas during dye adsorption 1, 10, 30, 60, and 150 min were less than 100.901, 97.492, 91.266, 99.451, and 96.144 µm in size, respectively. When the adsorption process was completed (namely 150 min), $d(0.1)$, $d(0.5)$, $d(0.9)$ and the volume mean diameter D[4,3] values were decreased.

3.1.3. Surface area and pore analyses

In order to ascertain the adsorption characteristics of adsorbent, several parameters such as total surface area, pore area, pore volume, pore diameter, and pore width of manure ash were determined by N$_2$ adsorption–desorption method. The BET specific surface area was 15.6593 m^2/g given by N$_2$ adsorption–desorption isotherms. The micropore surface area, calculated by the t-method, was 1.5403 m^2/g for manure ash.

Fig. 4 indicates that N$_2$ adsorption isotherms of manure ash exhibit a Type II sorption behavior in the classification of Brunauer, Deming, Deming and Teller. It is clearly seen that the same form of isotherms and hysteresis loop are seen in adsorbent. The large uptake of nitrogen is observed close to the saturation pressure, and this apparent step in adsorption branch
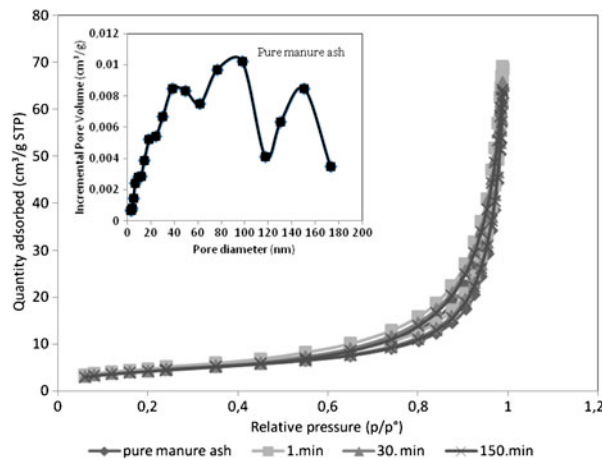
Fig. 4. Adsorption isotherms of nitrogen at 77 K of pure manure ash and after BY2 adsorption process.
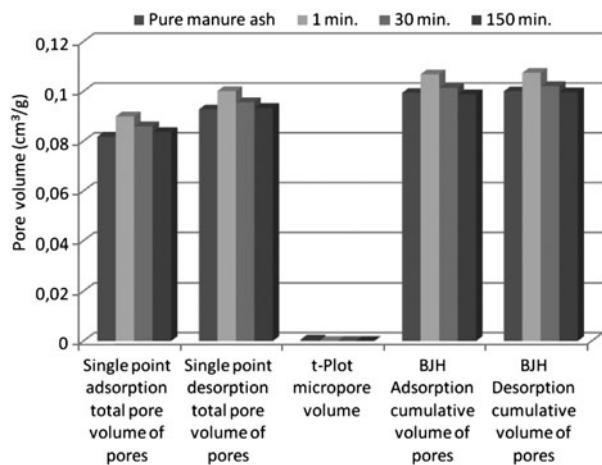

Fig. 5. Pore volumes changes of pure manure ash and after BY2 adsorption process.

with a sharp decline in the desorption branch implies the presence of mesoporosity [30].

Pore sizes are classified in accordance with the (IUPAC) classification, that is, micropores (diameter $(d) < 20\text{Å}$ (2 nm)), mesopores $(20\text{Å}$ (2 nm) $< d < 500\text{Å}$ (50 nm)), and macropores $d > 500\text{Å}$(50 nm) [31]. In Fig. 4, mostly mesopore structure of manure ash is seen clearly. Percentage of mesopores area is 90.2%. Additionally, in the adsorption process, it is likely that the multilayer adsorption will take place after completing monolayer adsorption. The weak interaction between adsorbent/adsorbate molecules resulted in the fovea shape of curves (Fig. 4) [32].

As seen in Fig. 4, the first abrupt increase in the adsorption capacity can be seen in the neighborhood at $p/p°$ of 0.60. This is due to the continuous progression from multilayer adsorption to capillary condensation in which the smaller pores become completely filled with liquid nitrogen. This occurs because the saturation vapor pressure in a small pore is reduced, according to Kelvin equation, by the effect of surface tension. It also indicates that, when $p/p°$ is higher than 0.90, the adsorption capacity hardly increases and that no pores with a large diameter exist. When $p/p°$ is higher than 0.010, there is an indication of the presence of micropores [33]. As seen in Fig. 5, while micropores volume is $0.000542\,cm^3/g$, micropores become completely filled with BY2 adsorption, and pore volume has been zero at 1, 30, and 150 min.

As seen in Table 3, BJH adsorption cumulative surface area of pores of manure ash increased with BY2 adsorption (150 min) from 14.981 to 15.984 m^2/g.

The Langmuir, BET, single point, and t-plot surface area of adsorbent used in our study are shown in Table 3. Also, changes in surface area of the adsorbent during the adsorption process (in 1, 30, and 150 min) are given in Table 3.

Table 3
Physical characteristics of manure ash before and after adsorption (obtained by applying the BET model to adsorption isotherms of nitrogen at 77 K)

Adsorbent	Single point P/P_0 (m^2/g)	BET surface area (m^2/g)	Langmuir surface area (m^2/g)	t-plot external surface area (m^2/g)	BJH adsorption cumulative surface area of pores (m^2/g)	BJH desorption cumulative surface area of pores (m^2/g)
Pure manure ash	15.1148	15.6593	21.5697	14.981	14.981	17.9041
1 min adsorption	16.4723	17.4788	24.4587	18.0494	17.988	22.2005
30 min adsorption	14.9357	15.8673	22.2120	16.1659	16.177	20.2954
150 min adsorption	14.6135	15.6732	22.0788	16.9460	15.984	19.1829

It was observed (Table 3) that the surface area of the manure ash increased with BY2 adsorption. After BY2 adsorption, BET surface area of adsorbent was especially increased at 1 min (can be clearly seen in Table 3). This indicates that adsorption occurs extensively in the first minutes. Langmuir, *t*-plot external surface area of adsorbent, and surface area of pores follow the same trend. This may be because of an increase in mesopore area and decrease in micropore area.

3.1.4. TEM

TEM images of the manure ash before and after the BY2 adsorption are presented in Fig. 6(a)–(d). The TEM image (Fig. 6(a)–(d)) shows that the large disorderness in the mesoporous shape and foam-like porous structure. Fig. 6(c) and (d) is the TEM image of manure ash after 30 and 150 min adsorption demonstrating clear porous structure.

3.2. Effect of temperature at different BY2 concentrations in batch studies

The initial dye concentration provides an important driving force to overcome all mass transfer resistance of BY2 between the aqueous and solid phases [34]. The temperature has two major effects on the adsorption process. Increasing the temperature is known to increase the rate of diffusion of the adsorbed molecules across the external boundary layer and the internal pores of the adsorbent particles, owing to the decrease in the viscosity of the solution. In addition, changing temperature will change the equilibrium capacity of the adsorbent for a particular adsorbate [20].

In this study, the effect of initial BY2 concentration on adsorption of the manure ash was investigated in the range of 10–150 mg/L of the initial dye concentration and the equilibrium uptake capacities (mg/g) and adsorption efficiencies (%) at 25, 45, and 60℃ are given in Fig. 7.

From this figure, it has been determined that the adsorption of BY2 has been found to increase with an increase in temperature from 25 to 45℃. The adsorption of BY2 on manure ash increased from 126.04 mg/g (60.6% removal) to 456.85 mg/g (89.09% removal) when temperature was increased from 25 to 45℃ at an initial concentration of 50 mg/L. The maximum equilibrium adsorption capacity values were determined as 729.05, 964.26, and 1200.3 mg/g for 150 mg/L initial BY2 concentration at 25, 35, and 45℃, respectively.
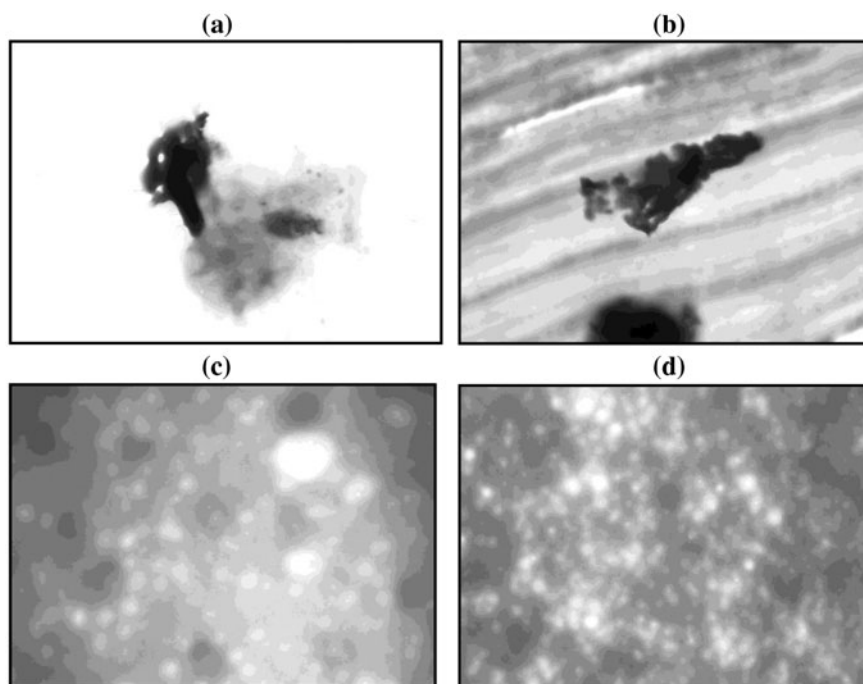

Fig. 6. TEM images of pure manure ash and after BY2 adsorption process. (a) Pure sample, (b) after 1 min adsorption, (c) after 30 min adsorption, and (d) after 150 min adsorption.
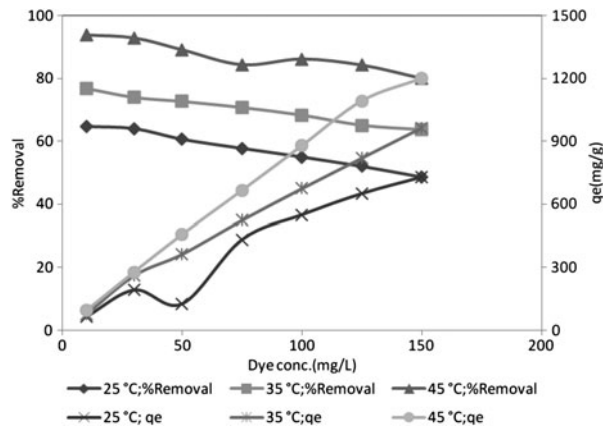
Fig. 7. Effect of temperature on BY2 adsorption efficiency and adsorption uptake at different dye concentrations (adsorbent concentration: 0.1 g/L, agitation speed: 240 rpm, pH 7.0).

3.3. Determination of thermodynamic parameters

Thermodynamic parameters, such as enthalpy change ($\Delta H°$), free energy change ($\Delta G°$), and entropy change ($\Delta S°$), can be estimated using equilibrium constants changing with temperature. The free energy change of the sorption reaction is given by the following Eqs. (6)–(8) [35].

$$K_D = \frac{\text{amount of dye in adsorbent}}{\text{amount of dye in solution}} = \frac{V}{W} \qquad (6)$$

$$\Delta G° = -RT \ln K_D \qquad (7)$$

where $\Delta G°$ is standard free energy change (J); R the universal gas constant, 8.314 J/(mol K), and the absolute temperature (K).

$$\Delta G° = \Delta H° - T\Delta S° \qquad (8)$$

The plot of $\Delta G°$ as a function of T (Fig. 8) a straight line from which $\Delta H°$ and $\Delta S°$ can be calculated from the slope and intercept, respectively. The thermodynamic parameters and Gibbs free energy change, $\Delta G°$, at different temperature and BY2 concentrations, are shown in Table 4.

As seen in Table 4, at all dye concentrations, the spontaneous nature of the ongoing adsorption process was ascertained by negative free energy $\Delta G°$ values, while the positive value of change in enthalpy ($\Delta H°$) suggested the endothermic nature of the process. The positive value of change in entropy $\Delta S°$ revealed the increased randomness during the adsorption process and provided excellent affinity of manure ash toward the BY2 molecules [18].
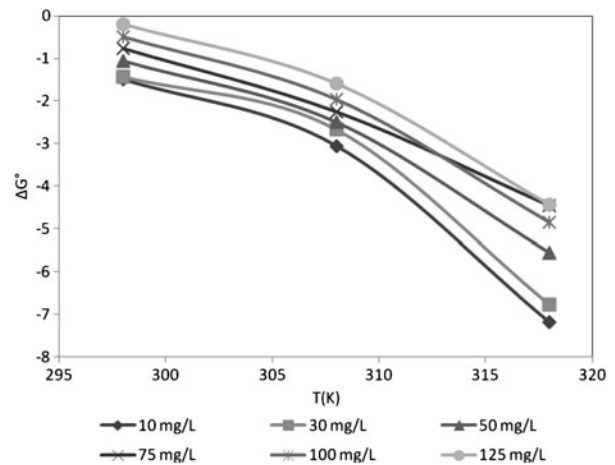

Fig. 8. $\Delta G°$ vs. T for the adsorption of BY2 by manure ash from aqueous solution at different dye concentrations.

Table 4
Thermodynamic parameters of manure ash at different initial BY2 concentrations at pH 7.0

BY2 conc. (mg/L)	$\Delta G°$ (kJ/mol)			$\Delta H°$ (kJ/mol)	$\Delta S°$ (J/mol K)
	298 K	308 K	318 K		
10	−1.49	−3.06	−7.19	83.75	284.6
30	−1.43	−2.67	−6.78	78.81	267.6
50	−1.07	−2.50	−5.55	65.99	224.1
75	−0.77	−2.26	−4.46	54.27	184.3
100	−0.49	−1.96	−4.84	64.45	217.1
125	−0.20	−1.59	−4.43	63.07	211.5

3.4. Adsorption isotherm studies

Adsorption properties and equilibrium data, adsorption isotherms, describe how pollutants interact with adsorbent materials and are very important for optimization of adsorption system [14]. An adsorption isotherm is characterized by certain constant values, which express the surface properties and affinity of the adsorbent and can also be used to compare the adsorptive capacities of the adsorbent for different pollutants [36].

In order to determine the mechanism of BY2 adsorption on the manure ash and evaluate the relationship between adsorption temperatures, the experimental data were applied to the Langmuir, Freundlich, D–R, Temkin, Frumkin, and Harkins–Jura isotherm equations. The constant parameters of the isotherm equations for this adsorption process were calculated by regression using linear form of the isotherm equations given in Table 5. The constant parameters and correlation coefficient (R^2) are summarized in Table 6.

According to Table 6, assessment of the results of model fitting to the adsorption of BY2 showed that Freundlich adsorption isotherm model best described the adsorption processes for all temperature; this was based on the high values of correlation coefficients R^2 (>0.98).

Table 5
Used in the adsorption isotherms and linear forms [36]

Adsorption isotherm	Linearized form
Langmuir	$\frac{C_e}{q_e} = \frac{1}{Q_0 K} + \frac{C_e}{Q_0}$
Freundlich	$\ln q_e = \ln K_f + \frac{1}{n} \ln C_e$
Temkin	$q_e = B \ln A + B \ln C_e$
Dubinin–Radushkevich	$\ln q_e = \ln q_m - K \in^2$ $E = \frac{1}{\sqrt{2K}}$
Harkins–Jura	$\frac{1}{q_e^2} = \frac{B}{A} - \frac{1}{A} \log C_e$
Frumkin	$\ln\left[\left(\frac{\theta}{1-\theta}\right)\frac{1}{C_e}\right] = \ln k + 2a\theta$

Table 6
Isotherm constants for BY2 sorption on ash of manure at different temperatures

Type	BY2		
	25℃	35℃	45℃
Langmuir isotherm			
Q_0 (mg/g)	1428.6	2000	1666.7
b (L/g)	0.014	0.017	0.08
R^2	0.9971	0.9721	0.9370
Freundlich isotherm			
K_f (L/g)	27.15	44.72	144.91
$1/n$	0.7833	0.7841	0.6564
R^2	0.9897	0.9893	0.9856
Temkin isotherm			
A (L/g)	0.277	2.52	1.46
B	219.32	275.78	289.62
R^2	0.9478	0.9271	0.9138
D–R isotherm			
K (mol^2/kJ^2)	5.10^{-5}	3.10^{-6}	3.10^{-7}
q_m (mg/g)	469.51	590.39	744.79
R^2	0.7976	0.8046	0.7928
E (kJ/mol)	1.00	0.41	1.29
Harkins–Jura			
A	5,000	10.000	16.666
B	1.5	2	1.17
R^2	0.7066	0.7002	0.6898
Frumkin			
a	1.292	1.088	0.681
$\ln k$	3.667	3.178	1.760
$-\Delta G$	9.085	8.14	4.65
R^2	0.8805	0.8924	0.7914

Furthermore, the Freundlich exponent $1/n$ gives an indication of the favorability of adsorption. The value of $1/n < 1.0$ represents a favorable adsorption condition. The value of $1/n$ obtained in the present study for BY2 is less than unity, indicating the favorable adsorption of BY2 onto manure ash [37].

The mean adsorption capacity q_m was found to be less than the Langmuir adsorption capacity Q_0 at all temperatures. This difference in adsorption capacity might be attributed to different assumptions taken into consideration while formulating these isotherms. The mean E value is useful in estimating the type of adsorption. An energy range 1–8 kJ/mol is indicative of physical adsorption, while that in 8–16 kJ/mol indicates chemisorptions [38]. The E values in the range 1–8 kJ/mol at 25 and 45℃ indicated physical adsorption.

The essential characteristics of the Langmuir isotherm parameters can be used to predict the affinity between the sorbate and sorbent using separation factor or dimensionless equilibrium parameter, "R_L", expressed as in Eq. (9):

$$R_L = \frac{1}{1 + bC_0} \tag{9}$$

where b is the Langmuir constant and C_0 is the initial concentration of BY2. The value of separation parameter R_L provides important information about the nature of adsorption. The value of R_L indicated the type of Langmuir isotherm to be irreversible ($R_L = 0$), favorable ($0 < R_L < 1$), linear ($R_L = 1$), or unfavorable ($R_L > 1$) [39]. Our data calculated from the experimental data and Eq. (9) showed that the value of R_L in all the cases lies between 0 and 1, and approached zero as C_0 increased (data not shown), indicating that dye adsorption on the manure ash is favorable.

Also, Table 6 shows the D–R, Temkin, Harkins–Jura, and Frumkin isotherm equations constant and its respective correlation coefficients. The low R^2 values of these models show their inapplicability for interpretation of experimental data.

3.5. Adsorption kinetic studies

3.5.1. Lagergren's pseudo-first-order model

The simples model used in the literature to fit the kinetics sorption experiments assume a Lagergren's pseudo-first-order model Eq. (10) [40]:

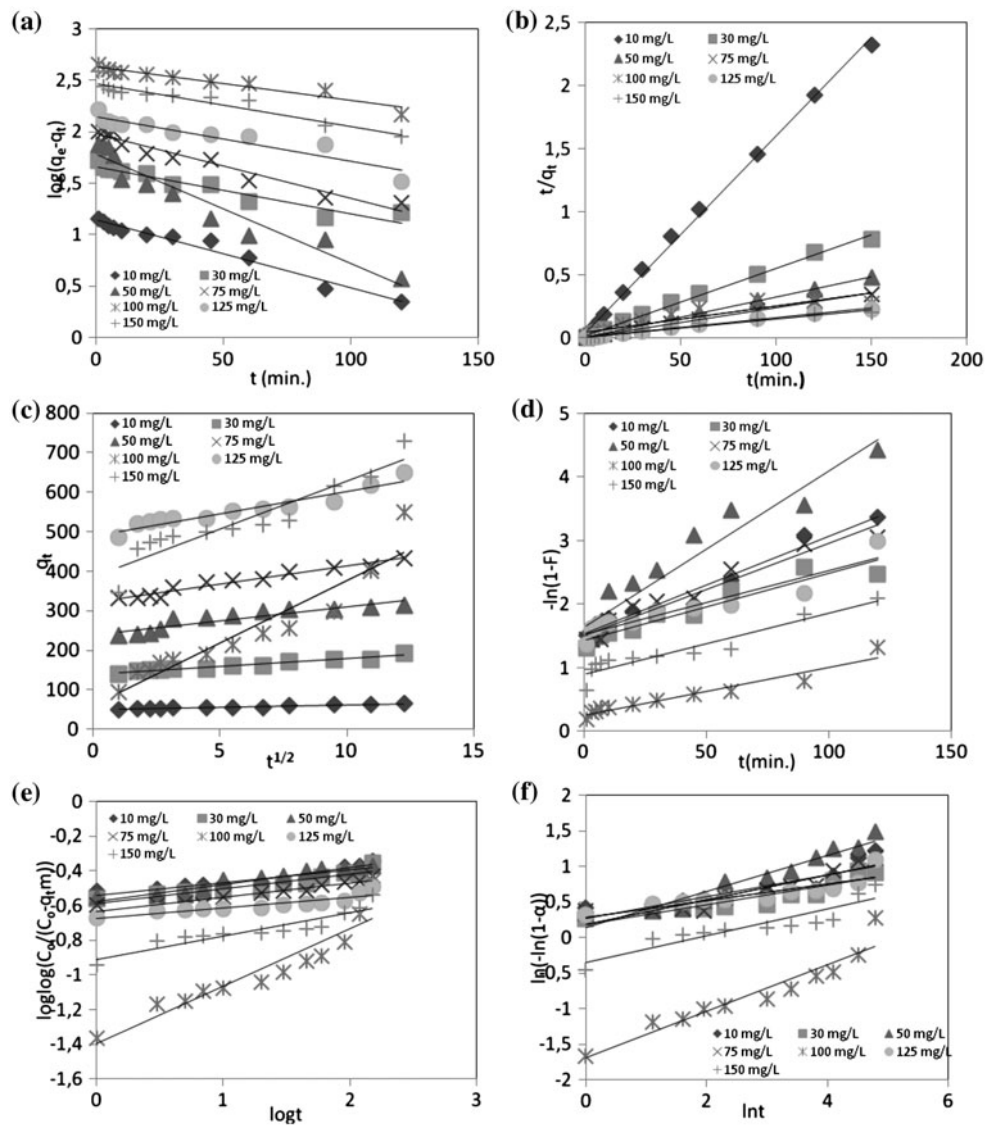$$\log(q_e - q_t) = \log q_e - \frac{k_1}{2.303} t \tag{10}$$

Fig. 9. Kinetic models for BY2 adsorption on manure ash at different initial concentrations at 25°C. (a) Lagergren's pseudo first-order kinetic model, (b) pseudo second-order kinetic model, (c) intra-particle diffusion model, (d) liquid-film diffusion model, (e) Bangham's equation, and (f) Avrami kinetic model.

where q_t (mg/g) is the amount of adsorbed dye on the adsorbent at time t and k_1 (1/min) is the rate constant of first-order adsorption. A straight line of log $(q_e - q_t)$ versus t suggests the applicability of this kinetic model. q_e and k_1 can be determined from the intercept and slope of the plot, respectively (Figs. 9(a), 10(a), and 11(a)).

3.5.2. The pseudo-second-order kinetic model

The pseudo-second-order kinetic model used in this study can be represented by the following Eq. (11):

$$\frac{t}{q_t} = \frac{1}{k_2 q_e^2} + \frac{1}{q_e} t \tag{11}$$

where k_2 (g/(mg/min)) is the rate constant of second-order adsorption and q_e and q_t are amounts of BY2 sorbed (mg/g) at equilibrium and at any time (t), respectively [40]. (In Figs. 9(b), 10(b), and 11(b).)

$$h = k_2 q_e^2 \tag{12}$$

where h is the initial sorption rate (mg(g min)) [41].

Fig. 10. Kinetic models for BY2 adsorption on manure ash at different initial concentrations at 35℃. (a) Lagergren's pseudo first-order kinetic model, (b) pseudo second-order kinetic model, (c) intra-particle diffusion model, (d) liquid-film diffusion model, (e) Bangham's equation, and (f) Avrami kinetic model.

3.5.3. Intra-particle diffusion model

The intra-particle diffusion model in Eq. (13) [42]:

$$q_t = k_t t^{1/2} + C \tag{13}$$

where k_t is the intra-particle diffusion rate constant (mg(g min$^{1/2}$)) and C is the intercept. The value of C relates to the thickness of the boundary layer. The larger C implies the greater effect of the boundary layer.

3.5.4. Liquid-film diffusion model

Liquid-film diffusion can be explained by the following Eqs. (14) and (15) [38]:

$$F = \frac{q_t}{q_e} \tag{14}$$

$$-\ln(1 - F) = k_{fd}t \tag{15}$$

where F is the fractional attainment of equilibrium at time t, and k_{fd} (1/min) is the adsorption rate constant for liquid-film diffusion.

3.5.5. Avrami kinetic model

Despite the Lagergren kinetic equations being used for most adsorption kinetic works, determination of some kinetic parameters, as possible changes of the
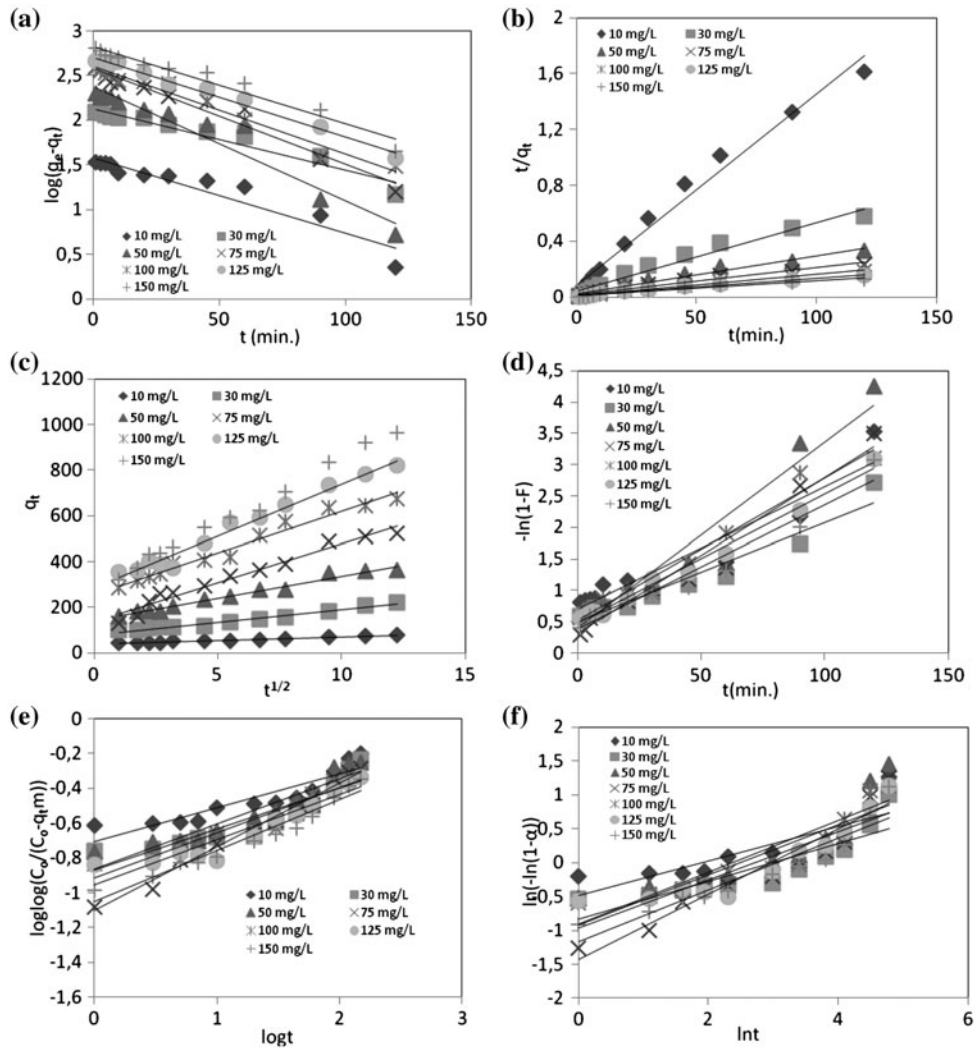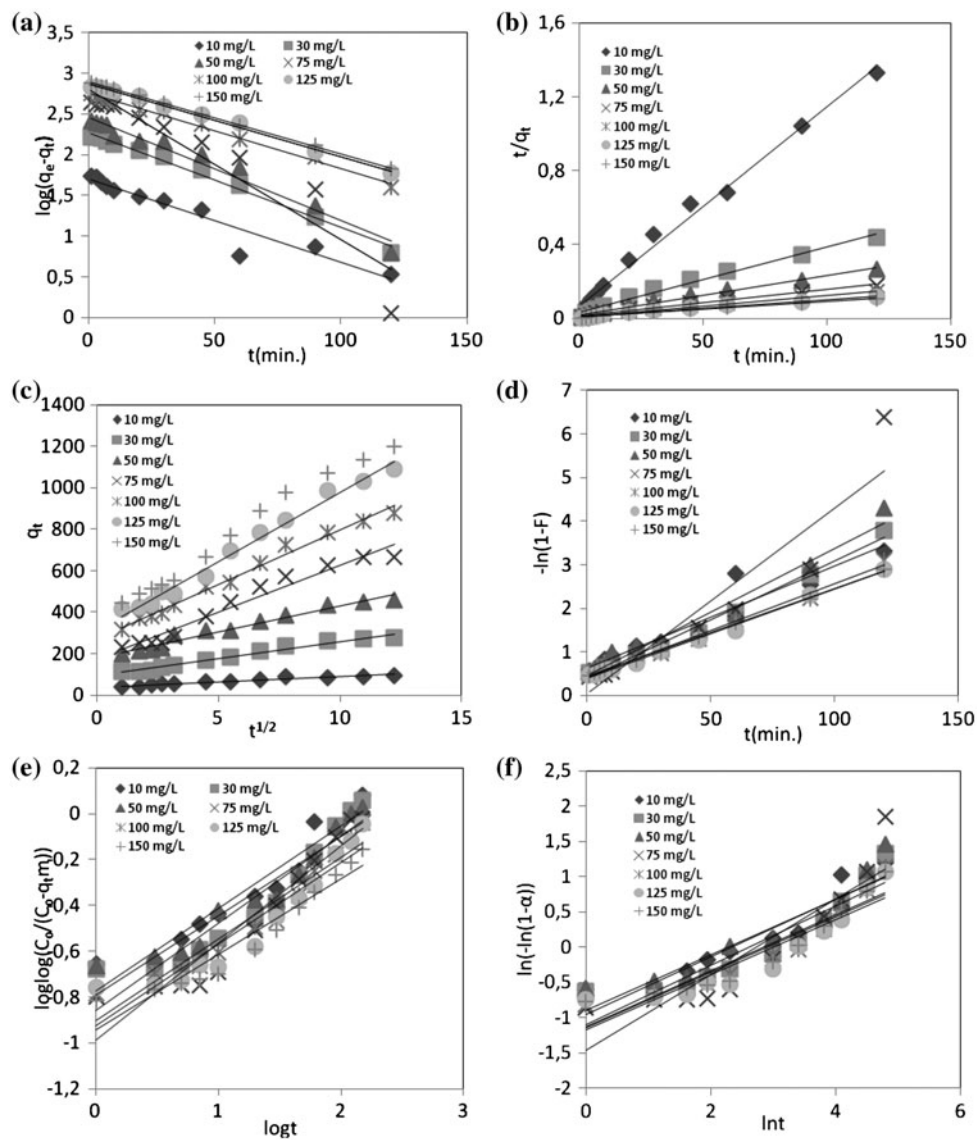
Fig. 11. Kinetic models for BY2 adsorption on manure ash at different initial concentrations at 45°C. (a) Lagergren's pseudo first-order kinetic model, (b) pseudo second-order kinetic model, (c) intra-particle diffusion model, (d) liquid-film diffusion model, (e) Bangham's equation, and (f) Avrami kinetic model.

adsorption rates in function of the initial concentration and the adsorption time, as well as the determination of fractionary kinetic orders, still lacks in the kinetic adsorption modelings. The adsorption should be visualized now using Avrami's exponential function shown in Eq. (16):

$$\ln\left(-\ln\left(1-\alpha\right)\right) = n\ln k_{av} + n\ln t \qquad (16)$$

where α is adsorption fraction at time t, k_{av} is the Avrami kinetic constant, and n is a constant which

can be relationed, first, to the adsorption mechanism (Figs. 9(f), 10(f), and 11(f)) [43].

3.5.6. Bangham's equation

Kinetic data were further used to know about the slow step occurring in the present adsorption system using Bangham's Eq. (17) [21]:

$$\log\log\left(\frac{C_0}{C_0 - q_t m}\right) = \log\left(\frac{k_0 m}{2.303 V}\right) + \infty \log t \qquad (17)$$

Table 7
Kinetic parameters for the adsorption of BY2 onto manure ash at different initial dye concentrations and temperatures

Kinetic model	25°C C_0 (mg/L)							35°C C_0 (mg/L)							45°C C_0 (mg/L)						
	10	30	50	75	100	125	150	10	30	50	75	100	125	150	10	30	50	75	100	125	150
$q_{e\text{-}exp}$ (mg/g)	64.78	191.99	303.02	432.84	549.96	650.36	729.15	76.8	261.8	363.18	524.08	674.8	820.1	964.26	93.82	278.55	456.85	665.44	878.7	1092.5	1200.3
Lagergren's pseudo first-order kinetic model																					
$q_{e1,cal}$ (mg/g)	13.84	45.81	60.62	95.96	425.4	141.1	296.82	38.22	133.91	239.28	382.74	398.02	504.31	656.60	49.98	186.15	288.34	633.29	570.56	732.82	776.25
k_1 (1/min)	0.015	0.011	0.025	0.015	0.008	0.010	0.009	0.019	0.016	0.029	0.029	0.022	0.020	0.020	0.023	0.027	0.029	0.043	0.021	0.021	0.020
R^2	0.9712	0.9220	0.9281	0.9481	0.9302	0.8804	0.8956	0.9029	0.9400	0.9356	0.9612	0.9747	0.9865	0.9558	0.9223	0.9903	0.9684	0.8936	0.9921	0.9932	0.9990
Pseudo second-order kinetic model																					
$q_{e,cal}$ (mg/g)	64.10	185.2	312.5	434.78	476.2	625	714.29	72.99	204.08	370.37	526.32	666.67	769.23	909.1	92.59	285.7	454.55	714.28	833.33	1111.11	1111.11
k_2 (g/(mg min))	0.006	0.0018	0.002	0.0009	0.00009	0.0005	0.0002	0.0023	0.00056	0.00032	0.00018	0.00019	0.00016	0.00011	0.0017	0.0004	0.0003	0.00012	0.00014	0.00009	0.0001
h (mg/(g min))	24.65	61.35	192.31	169.49	20.28	212.76	103.09	12.24	23.36	45.25	50.00	85.47	94.34	92.57	14.97	31.84	62.89	62.50	95.24	106.38	126.58
R^2	0.9979	0.9958	0.9997	0.9982	0.8363	0.9950	0.9796	0.9818	0.9693	0.9784	0.9746	0.9838	0.9843	0.9704	0.9916	0.9861	0.9881	0.9847	0.9836	0.9799	0.9852
Intra-particle diffusion model																					
k_i (mg/g min$^{1/2}$)	1.2079	3.9866	6.9488	9.2129	31.552	11.234	24.408	3.1028	10.981	19.31	34.071	36.618	45.411	56.678	5.0309	16.598	25.036	45.512	52.349	66.36	72.112
C	49.42	138.25	240.04	320.57	61.91	490.09	384.77	37.96	79.50	141.97	136.05	254.74	285.75	280.12	38.182	92.796	178.71	171.88	272.42	313.28	361.42
R^2	0.9793	0.9592	0.8486	0.9582	0.8847	0.9084	0.8744	0.9704	0.9711	0.9790	0.9653	0.9734	0.9796	0.9928	0.9540	0.9784	0.9651	0.9605	0.9884	0.9875	0.9880
Liquid-film diffusion model																					
k_{fd}	0.0153	0.0105	0.0245	0.0146	0.0075	0.01	0.0096	0.0195	0.0158	0.0295	0.0248	0.0226	0.0205	0.0198	0.0234	0.0268	0.0291	0.0213	0.0425	0.0204	0.0202
R^2	0.9712	0.9220	0.9281	0.9481	0.9302	0.8804	0.8956	0.9029	0.9400	0.9356	0.9612	0.9747	0.9865	0.9558	0.9223	0.9903	0.9684	0.9920	0.8936	0.9932	0.9990
Avrami kinetic model																					
k_{av}	6.04	3.66	1.75	2.99	0.006	12.39	0.15	0.012	0.05	0.09	0.05	0.08	0.07	0.046	0.101	0.073	0.096	0.065	0.058	0.050	0.055
n	0.1531	0.1391	0.2544	0.1725	0.3273	0.1160	0.1879	0.2549	0.2767	0.3813	0.4808	0.3681	0.3543	0.3797	0.3941	0.4188	0.4081	0.5353	0.3971	0.3895	0.3915
R^2	0.7813	0.8613	0.9249	0.8698	0.9084	0.7719	0.8352	0.7311	0.7629	0.7863	0.9226	0.8529	0.8339	0.8782	0.9036	0.8556	0.8611	0.8259	0.8924	0.8559	0.8841
Bangham's equation																					
k_0	6614.4	5970.3	6114.9	5367.8	930.24	4864	2817.1	4538.3	3088.8	3164.4	1831.1	2793.2	2543.9	2055.4	3868.1	3195.9	3707.6	2376.8	2882.7	2739.1	2628.4
α	0.075	0.084	0.098	0.082	0.331	0.062	0.137	0.194	0.238	0.260	0.366	0.259	0.260	0.292	0.362	0.382	0.348	0.429	0.357	0.356	0.329
R^2	0.8698	0.8672	0.9365	0.9051	0.8717	0.8193	0.8428	0.8391	0.8295	0.9080	0.9747	0.9253	0.8953	0.9507	0.9349	0.9023	0.9238	0.9123	0.9297	0.8951	0.9256

where V is the volume of solution (mL), q_t (mg/g) is the amount of adsorbate retained at t, and α (<1) and k_0 are constants (Figs. 9(e), 10(e), and 11(e)).

As seen Table 7, it can be seen that the values of correlation coefficient for pseudo-second order are relatively higher than those for other kinetic models. Additionally, experimental q_e values are very close to the calculated q_e values for pseudo-second-order kinetic model. These results implied that the adsorption of BY2 could be best described by the pseudo-second-order model.

The calculated Avrami constants (n and k_{Av}) are different from 25 to 45℃. In this manner, for this temperature range, the adsorption of the BY2 seems to present both temperature and dye concentration dependence in relation to the adsorption kinetic parameters. Table 7 shows the numerical values of the models parameters. In general, the kinetic constants (k_{Av}) decrease when the BY2 concentration increases.

In intra-particle diffusion models, the results showed that the plots presented a multilinearity which indicated that two or more steps occurred in the process. The R^2 values for this diffusion model were between 0.8486 and 0.9928. As seen Figs. 9(c), 10(c), and 11(c), it can be also observed that the plots did not pass through the origin; this was indicative of some degree of boundary layer control and this further showed that the intra-particle diffusion was not the only rate-limiting step, but other processes might control the rate of adsorption [44]. The rate constants (k_t) obtained at different temperatures increased with increasing dye concentration.

Liquid film diffusion model in Figs. 9(d), 10(d), and 11(d) were found to be linear ($R^2 = 0.8804 – 0.9990$) at different BY2 concentrations of each temperature, thereby confirming the applicability of the model. The plots, however, did not pass through the origin indicating that the liquid-film diffusion was not the predominant mechanism for BY2 adsorption onto manure ash [38].

As seen Eq. (17), the double logarithmic plot according to above equation did not yield perfect linear curves for BY2 removal by manure ash showing that the diffusion of adsorbate into pores of the sorbent is not the only rate-controlling step. With increase in the contact time, the effect of diffusion process on overall sorption could be ignored. It may be that both film and pore diffusions are involved in the removal process to different extent [21].

3.6. Column studies

3.6.1. Effect of different bed depths on breakthrough curve

The effect of bed depth on the BY2 adsorption by manure ash was investigated by varying the bed depth

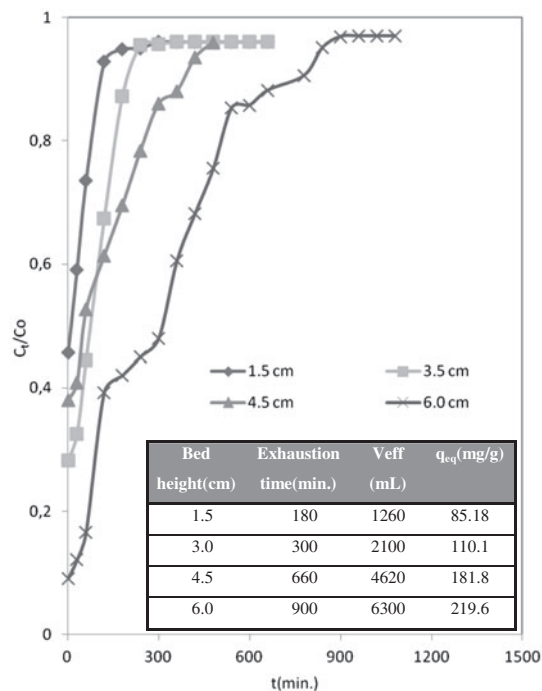| Bed height(cm)	Exhaustion time(min.)	Veff (mL)	q_{eq}(mg/g)
1.5	180	1260	85.18
3.0	300	2100	110.1
4.5	660	4620	181.8
6.0	900	6300	219.6

Fig. 12. Breakthrough curves for BY2 adsorption with manure ash at different bed depths (initial dye conc.: 300 mg/L, flow rate: 7 mL/min).

from 1.5 to 6 cm at constant initial dye concentrations (300 mg/L), flow rate (7 mL/min). The bed depths of column was packed to approximately 1.5, 3, 4.5, and 6 cm corresponding to 0.6852, 1.598, 2.056, and 2.741 g of adsorbent, respectively. The breakthrough curves at different bed depths are shown in Fig. 12.

As seen shown in Fig. 12, it is clear that as the bed depths increased, both the exhaustion time and effluent volume (V_{eff}) increased. With increase in bed depth, the V_{eff} increased which might be due to the more contact time. This was due to increase in the specific surface of the adsorbents which supplies more fixation binding sites. Then, it followed that a delayed breakthrough of the pollutant led to an increase in the volume of solution treated. The increase in adsorption with that in bed depths was due to the increase in absorbents doses in larger beds which provided greater surface area. When the bed depths was reduced, axial dispersion phenomena predominated in the mass transfer and reduced the diffusion of dye ions. The dye ions did not have enough time to diffuse into the whole of the adsorbents mass [24].

3.6.2. Effect of different initial BY2 concentrations on breakthrough curve

The effect of initial BY2 concentrations on breakthrough performance of the manure ash was studied

by varying the initial dye concentration from 100 to 300 mg/L. For this experiment, the bed depth and flow rate were kept constant at 4.5 cm and 1.8 mL/min, respectively. The effect of initial BY2 concentration on the breakthrough curves is shown in Fig. 13.

A decreased initial dye concentration gave a later breakthrough curve and increased the treated volume. Increasing the dye concentration leads to a decrease in the value of the breakthrough time from 1620 to 1320 min. This can be explained by the fact that at the greater concentration gradient caused a faster transport due to an increased diffusion coefficient or mass transfer coefficient [45]. Also, by increasing the initial dye concentration, the volume of solution treated before breakthrough point was considerably reduced. This is due to the fact that at higher dye concentrations the column bed is easily saturated; thereby the breakthrough time is reached faster. The main driving force for the adsorption process is the concentration difference between the solute in the solution and the adsorbed material on the adsorbent. This explains why more adsorbed dye quantities were obtained at higher dye concentrations [10].

It is clear that the maximum bed capacity of BY2 decreased with the increase in the initial dye concentration. For tested different initial dye concentration,

maximum bed capacities at 100, 150, 200, and 300 mg/L BY2 concentrations were 45.73, 61.83, 79.44, and 113.23 mg/g, respectively.

3.7. Modeling of the breakthrough curves

3.7.1. Thomas model

The maximum bed capacity of an adsorption column is needed in design. The Thomas model is used to fulfill the purpose. The Thomas solution is one of the most general and widely used methods in column performance theory. The model has the following Eq. (18) [46]:

$$\ln\left(\frac{C_0}{C_t} - 1\right) = \frac{k_{TH}q_0 X}{Q} - k_{TH}C_0 t \tag{18}$$

where k_{TH} is the Thomas rate constant (mL/(min mg)), q_0 the maximum solid phase concentration of the solute (mg/g), V_{eff} the effluent volume (mL), X the mass of adsorbent (g), and Q the flow rate (mL/min).

The Thomas model was applied to the experimental data with respect to the initial BY2 concentration and bed depth. The model parameters were determined from the linear plot (data not shown) of Eq. (18) and are presented in Table 8. Table 8 shows that k_{TH} generally decreased with increasing bed depth and initial BY2 concentration. Similarly, q_0 increased with increasing bed depth and the initial dye concentration. The reason is that the driving force for adsorption is the concentration difference between the dye on the adsorbent and the dye in the solution [47]. From Table 8, it is seen that values of determined coefficients (R^2) range from 0.8523 to 0.9828. The
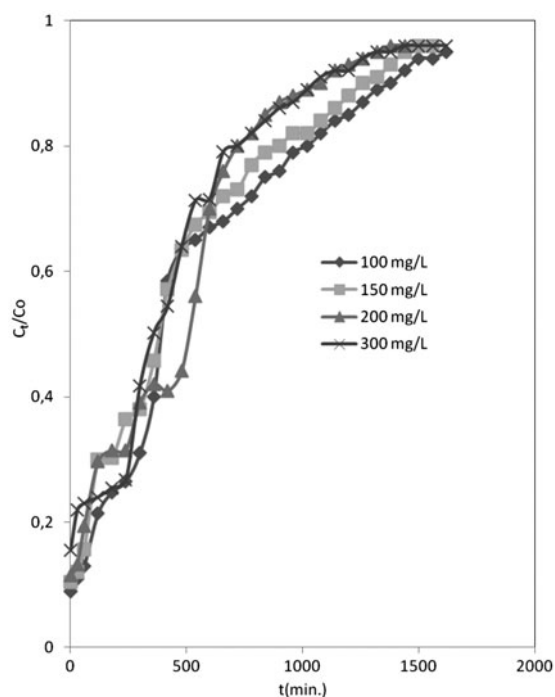
Fig.13. Breakthrough curves for BY2 adsorption with manure ash at different initial dye concentration (bed depth: 4.5 cm, flow rate: 1.8 mL/min, pH 7.0).

Table 8
Thomas model parameters at different conditions using linear regression analysis

Initial BY2 conc. (mg/L)	Bed depth (cm)	Flow rate (mL/ min)	$q_{e,exp}$ (mg/ g)	q_0 (mg/ g)	k_{TH} (mL/ min mg) $\times 10^{-5}$	R^2
100	4.5	1.8	45.73	45.18	2.80	0.9457
150	4.5	1.8	61.83	58.51	1.93	0.9588
200	4.5	1.8	79.44	76.09	1.75	0.9755
300	4.5	1.8	113.23	102.95	1.13	0.9712
300	1.5	7.0	85.18	82.24	3.80	0.8523
300	3.5	7.0	110.1	84.72	4.40	0.9395
300	4.5	7.0	181.8	149.33	2.10	0.9828
300	6.0	7.0	219.6	230.64	1.93	0.9656

Thomas model is suitable for adsorption processes where the external and internal diffusions will not be the limiting step [47].

3.7.2. Adam's–Bohart model

Adam's–Bohart model is based on the surface reaction theory and it assumes that equilibrium is not instantaneous; therefore, the rate of the sorption is proportional to the fraction of sorption capacity still remains on the sorbent. The Adam's–Bohart model in Eq. (19) is used for the description of the initial part of the breakthrough curve [48].

$$\ln\left(\frac{C_t}{C_0}\right) = k_{AB}C_0 t - k_{AB}N_0\frac{Z}{U_0} \tag{19}$$

where C_0 and C_t are the inlet and effluent dye concentrations (mg/L), respectively. Z is the depth of the column (cm), U_0 is the superficial velocity (cm/min), N_0 is saturation concentration in the Adams–Bohart model (mg/L), and k_{AB} is the mass transfer coefficient (L(mg min)). The range of t should be considered from the beginning to the end of breakthrough. A straight line was attained for this system by plotting $\ln(C_t/C_0)$ against t, which gives the value of k_{AB} from the slope of the line.

Calculated from the linear regression analysis, the values of k_{AB} and N_0 are given in Table 9 along with their correlation coefficients (R^2). Contrary to expectations, an increase in the inlet dye concentration decreased the bed capacity, N_0, of the column from 5.49 to 4.82 g/L. Similar results have been reported for the adsorption of dyes on chitosan [11]. It is likely that BY2 can aggregate at higher dye concentrations [11,49], which could block the pores; therefore, the

sites within the micropore of adsorbent could not be utilized [11].

As shown in Table 9, the values of k_{AB} usually does not change with increase of initial dye concentration, but increased with increasing bed depth (except for 1.5 cm). It was indicated that the overall system kinetics was dominated by external mass transfer in the initial part of adsorption in the column [45].

3.7.3. Yoon–Nelson model

Yoon–Nelson model is based on the assumption that the rate of decrease in the probability of adsorption for each adsorbate molecule is proportional to the probability of adsorbate adsorption and the probability of adsorbate breakthrough on the adsorbent. The Yoon–Nelson equation regarding to a single component system is expressed as in Eq. (20) [46]:

$$\ln\left(\frac{C_t}{C_0 - C_t}\right) = k_{YN}t - \tau k_{YN} \tag{20}$$

where k_{YN} is the rate constant (L/min), τ the time required for 50% adsorbate breakthrough (min), and t the breakthrough time (min). The kinetic coefficient k_{YN} and τ can be determined from a plot of $\ln\left[C_t/(C_0-C_t)-1\right]$ against t at a given adsorption conditions. If the theoretical model accurately characterizes the experimental data, this plot will result in a straight line with slope of k_{YN} and intercept τk_{YN}.

The values of k_{YN} and τ are listed in Table 10. The k_{YN} values τ values time for 50% breakthrough) increased with increasing bed depth. The data in Table 10 also indicated that τ values are very similar to experimental results. However, the value of τ

Table 9
Adam's–Bohart parameters at different conditions using linear regression analysis

Initial BY2 conc. (mg/L)	Bed depth (cm)	Flow rate (mL/min)	N_0 (g/L)	k_{AB} (L/mgmin) × 10^{-6}	R^2
100	4.5	1.8	5.49	4.0	0.7340
150	4.5	1.8	5.07	4.0	0.7315
200	4.5	1.8	4.98	4.3	0.8221
300	4.5	1.8	4.82	4.0	0.8122
300	1.5	7.0	–	7.3	0.7139
300	3.5	7.0	7.99	0.12	0.8330
300	4.5	7.0	9.07	6.3	0.9551
300	6.0	7.0	6.87	7.3	0.7565

Table 10
Yoon–Nelson model parameters at different conditions using linear regression analysis

Initial BY2 conc. (mg/L)	Bed depth (cm)	Flow rate (mL/min)	τ_{exp} (min)	τ_{mod} (min)	k_{YN} (L/min)	R^2
100	4.5	1.8	480	526	0.0114	0.8523
150	4.5	1.8	450	468	0.0131	0.9395
200	4.5	1.8	400	449	0.0064	0.9828
300	4.5	1.8	360	394	0.0058	0.9656
300	1.5	7.0	50	27	0.0030	0.9350
300	3.5	7.0	80	65	0.0030	0.9502
300	4.5	7.0	180	144	0.0036	0.9756
300	6.0	7.0	320	300	0.0035	0.9726

significantly decreased as the initial dye concentration increased, because the saturation of the column occurred more rapidly [45]. On the other hand, with the increase in the dye concentration, the values of k_{YN} (except for 100 mg/L).

In a comparison of values of R^2, both the Thomas and Yoon–Nelson models can be used to predict adsorption performance for adsorption of BY2 in a fixed-bed column.

4. Conclusion

The results showed that manure ash can be used as sorbents for the effective removal of BY2 from aqueous solutions. The specific surface areas, pore size, and pore-size distributions of the samples were fully characterized. The analysis by FTIR further revealed that functional groups (bonded O–H groups, carboxyl groups, alkane groups, S–OR esters, N–H stretching, $-SO_3$ stretching, C–O stretching, and $-CN$ stretching) on manure ash would be the active binding sites for the adsorption of the studied dye. The adsorption efficiency of BY2 onto the manure ash was increased with increasing temperature. The six kinetic models for experimental data were applied. The experimental data fitted very well the pseudo-second-order kinetic model. The negative value of free energy indicates that the process is spontaneous and the positive values of entropy as well as enthalpy indicate higher affinity of the material for BY2. The adsorption process is determined to be endothermic. The adsorption data fitted well to Langmuir isotherm model. Fixed-bed adsorption systems were found to perform better for BY2 uptake by manure ash at a lower initial dye concentrations and higher bed depth. The adsorption data were fitted to three well-established fixed-bed adsorption models namely, Adam's–Bohart, Thomas, and Yoon–Nelson models. For BY2 adsorption, the column data were fitted well to the Thomas and Yoon–Nelson models. The present work shows that manure ash can be effectively used as a low-cost adsorbent for the removal of BY2 from wastewater.

References

[1] A. Saeed, M. Sharif, M. Iqbal, Application potential of grapefruit peel as dye sorbent: Kinetics, equilibrium and mechanism of crystal violet adsorption, J. Hazard. Mater. 179 (2010) 564–572.

[2] B. Balci, O. Keskinkan, M. Avci, Use of BDST and an ANN model for prediction of dye adsorption efficiency of *Eucalyptus camaldulensis* barks in fixed-bed system, Expert Syst. Appl. 38 (2011) 949–956.

[3] P. Pimol, M. Khanidtha, P. Prasert, Influence of particle size and salinity on adsorption of basic dyes by agricultural waste: Dried seagrape (*Caulerpa lentillifera*), J. Environ. Sci. 20 (2008) 760–768.

[4] D. Salari, A. Niaei, S. Aber, M.H. Rasoulifard, The photooxidative destruction of C.I. Basic Yellow 2 using $UV/S_2O_8^{2-}$ Process in a rectangular continuous photoreactor, J. Hazard. Mater. 166 (2009) 61–66.

[5] E. Eren, B. Afsin, Investigation of a basic dye adsorption from aqueous solution onto raw and pre-treated bentonite surfaces, Dyes Pigm. 76 (2008) 220–225.

[6] X. Wu, D. Wu, R. Fu, W. Zeng, Preparation of carbon aerogels with different pore structures and their fixed bed adsorption properties for dye removal, Dyes Pigm. 95 (2012) 689–694.

[7] J. Galán, A. Rodríguez, J.M. Gómez, S.J. Allen, G.M. Walker, Reactive dye adsorption onto a novel mesoporous carbon, Chem. Eng. J. 219 (2013) 62–68.

[8] V.K. Gupta, B. Gupta, A. Rastogi, S. Agarwal, A. Nayak, A comparative investigation on adsorption performances of mesoporous activated carbon prepared from waste rubber tire and activated carbon for a hazardous azo dye—Acid Blue 113, J. Hazard. Mater. 186 (2011) 891–901.

[9] P. Liao, Z. Malik Ismael, W. Zhang, S. Yuan, M. Tong, K. Wang, J. Bao, Adsorption of dyes from aqueous solutions by microwave modified bamboo charcoal, Chem. Eng. J. 195–196 (2012) 339–346.

[10] A. Goshadrou, A. Moheb, Continuous fixed bed adsorption of C.I. Acid Blue 92 by exfoliated graphite: An experimental and modeling study, Desalination 269 (2011) 170–176.

[11] J. Barron-Zambrano, A. Szygula, M. Ruiz, A.M. Sastre, E. Guibal, Biosorption of Reactive Black 5 from aqueous solutions by chitosan: Column studies, J. Environ. Manage. 91 (2010) 2669–2675.

[12] W. Li, Q. Yue, P. Tu, Z. Ma, B. Gao, J. Li, X. Xu, Adsorption characteristics of dyes in columns of activated carbon prepared from paper mill sewage sludge, Chem. Eng. J. 178 (2011) 197–203.

[13] D. Sidiras, F. Batzias, E. Schroeder, R. Ranjan, M. Tsapatsis, Dye adsorption on autohydrolyzed pine sawdust in batch and fixed-bed systems, Chem. Eng. J. 171 (2011) 883–896.

[14] A.R. Tehrani-Bagha, H. Nikkar, N.M. Mahmoodi, M. Markazi, F.M. Menger, The sorption of cationic dyes onto kaolin: Kinetic, isotherm and thermodynamic studies, Desalination 266 (2011) 274–280.

[15] M.T. Sulak, E. Demirbas, M. Kobya, Removal of Astrazon Yellow 7GL from aqueous solutions by adsorption onto wheat bran, Bioresour. Technol. 98 (2007) 2590–2598.

[16] H. Pekkuz, İ. Uzun, F. Güzel, Kinetics and thermodynamics of the adsorption of some dyestuffs from aqueous solution by poplar sawdust, Bioresour. Technol. 99 (2008) 2009–2017.

[17] A. Olgun, N. Atar, Equilibrium and kinetic adsorption study of Basic Yellow 28 and Basic Red 46 by a boron industry waste, J. Hazard. Mater. 161 (2009) 148–156.

[18] A. Mittal, D. Jhare, J. Mittal, Adsorption of hazardous dye Eosin Yellow from aqueous solution onto waste material De-oiled Soya: Isotherm, kinetics and bulk removal, J. Mol. Liq. 179 (2013) 133–140.

[19] S.J. Allen, G. McKay, J.F. Porter, Adsorption isotherm models for basic dye adsorption by peat in single and

binary component systems, J. Colloid Interface Sci. 280 (2004) 322–333.

[20] N. Barka, A. Assabbane, A. Nounah, L. Laanab, Y.A. Ichou, Removal of textile dyes from aqueous solutions by natural phosphate as a new adsorbent, Desalination 235 (2009) 264–275.

[21] I.D. Mall, V.C. Srivastava, N.K. Agarwal, Adsorptive removal of Auramine-O: Kinetic and equilibrium study, J. Hazard. Mater. 143 (2007) 386–395.

[22] E. Malkoc, Y. Nuhoglu, Removal of Ni(II) ions from aqueous solutions using waste of tea factory: Adsorption on a fixed-bed column, J. Hazard. Mater. 135 (2006) 328–336.

[23] Z. Aksu, F. Gönen, Biosorption of phenol by immobilized activated sludge in a continuous packed bed: Prediction of breakthrough curves, Process Biochem. 39 (2004) 599–613.

[24] X. Luo, Z. Deng, X. Lin, C. Zhang, Fixed-bed column study for Cu^{2+} removal from solution using expanding rice husk, J. Hazard. Mater. 187 (2011) 182–189.

[25] N.A. Travlou, G.Z. Kyzas, N.K. Lazaridis, E.A. Deliyanni, Graphite oxide/chitosan composite for reactive dye removal, Chem. Eng. J. 217 (2013) 256–265.

[26] M. Gohari, S.N. Hosseini, S. Sharifnia, M. Khatami, Enhancement of metal ion adsorption capacity of Saccharomyces cerevisiae's cells by using disruption method, J. Taiwan Inst. Chem. Eng. 44 (2013) 637–645.

[27] M. Torab-Mostaedi, M. Asadollahzadeh, A. Hemmati, A. Khosravi, Equilibrium, kinetic, and thermodynamic studies for biosorption of cadmium and nickel on grapefruit peel, J. Taiwan Inst. Chem. Eng. 44 (2013) 295–302.

[28] B. Singha, S.K. Das, Adsorptive removal of Cu(II) from aqueous solution and industrial effluent using natural/agricultural wastes, Colloids Surf., B 107 (2013) 97–106.

[29] A. Pirkarami, M.E. Olya, N. Yousefi Limaee, Decolorization of azo dyes by photo electro adsorption process using polyaniline coated electrode, Prog. Org. Coat. 76 (2013) 682–688.

[30] Y. Park, G.A. Ayoko, R.L. Frost, Characterisation of organoclays and adsorption of p-nitrophenol: Environmental application, J. Colloid Interface Sci. 360 (2011) 440–456.

[31] V.C. Srivastava, I.D. Mall, I.M. Mishra, Adsorption of toxic metal ions onto activated carbon: Study of sorption behaviour through characterization and kinetics, Chem. Eng. Process. 47 (2008) 1269–1280.

[32] L. Wang, L. Chen, H.L. Wang, D.L. Liao, The adsorption refrigeration characteristics of alkaline-earth metal chlorides and its composite adsorbents, Renewable Energy 34 (2009) 1016–1023.

[33] S. Chen, R. Wang, Surface area, pore size distribution and microstructure of vacuum getter, Vacuum 85 (2011) 909–914.

[34] Y. Nuhoglu, E. Malkoc, Thermodynamic and kinetic studies for environmentaly friendly Ni(II) biosorption using waste pomace of olive oil factory, Bioresour. Technol. 100 (2009) 2375–2380.

[35] A.K. Bhattacharya, S.N. Mandal, S.K. Das, Adsorption of Zn(II) from aqueous solution by using different adsorbents, Chem. Eng. J. 123 (2006) 43–51.

[36] E. Malkoc, Y. Nuhoglu, Determination of kinetic and equilibrium parameters of the batch adsorption of Cr(VI) onto waste acorn of *Quercus ithaburensis*, Chem. Eng. Process. 46 (2007) 1020–1029.

[37] R. Ahmad, R. Kumar, S. Haseeb, Adsorption of Cu^{2+} from aqueous solution onto iron oxide coated eggshell powder: Evaluation of equilibrium, isotherms, kinetics, and regeneration capacity, Arab. J. Chem. 5 (2012) 353–359.

[38] T.A. Khan, S. Dahiya, I. Ali, Use of kaolinite as adsorbent: Equilibrium, dynamics and thermodynamic studies on the adsorption of Rhodamine B from aqueous solution, Appl. Clay Sci. 69 (2012) 58–66.

[39] P. SenthilKumar, S. Ramalingam, V. Sathyaselvabala, S.D. Kirupha, S. Sivanesan, Removal of copper(II) ions from aqueous solution by adsorption using cashew nut shell, Desalination 266 (2011) 63–71.

[40] V.M. Vučurović, R.N. Razmovski, M.N. Tekić, Methylene blue (cationic dye) adsorption onto sugar beet pulp: Equilibrium isotherm and kinetic studies, J. Taiwan Inst. Chem. Eng. 43 (2012) 108–111.

[41] E. Malkoc, Ni(II) removal from aqueous solutions using cone biomass of *Thuja orientalis*, J. Hazard. Mater. 137 (2006) 899–908.

[42] E. Alver, A.Ü. Metin, Anionic dye removal from aqueous solutions using modified zeolite: Adsorption kinetics and isotherm studies, Chem. Eng. J. 200–202 (2012) 59–67.

[43] E.C.N. Lopes, F.S.C. dos Anjos, E.F.S. Vieira, A.R. Cestari, An alternative Avrami equation to evaluate kinetic parameters of the interaction of Hg(II) with thin chitosan membranes, J. Colloid Interface Sci. 263 (2003) 542–547.

[44] G. Crini, Kinetic and equilibrium studies on the removal of cationic dyes from aqueous solution by adsorption onto a cyclodextrin polymer, Dyes Pigm. 77 (2008) 415–426.

[45] S. Chen, Q. Yue, B. Gao, Q. Li, X. Xu, K. Fu, Adsorption of hexavalent chromium from aqueous solution by modified corn stalk: A fixed-bed column study, Bioresour. Technol. 113 (2012) 114–120.

[46] E. Malkoc, Y. Nuhoglu, Y. Abali, Cr(VI) adsorption by waste acorn of Quercus ithaburensis in fixed beds: Prediction of breakthrough curves, Chem. Eng. J. 119 (2006) 61–68.

[47] A.A. Ahmad, B.H. Hameed, Fixed-bed adsorption of reactive azo dye onto granular activated carbon prepared from waste, J. Hazard. Mater. 175 (2010) 298–303.

[48] E. Malkoc, Y. Nuhoglu, M. Dundar, Adsorption of chromium(VI) on pomace—An olive oil industry waste: Batch and column studies, J. Hazard. Mater. 138 (2006) 142–151.

[49] E. Guibal, J. Roussy, Coagulation and flocculation of dye-containing solutions using a biopolymer (Chitosan), React. Funct. Polym. 67 (2007) 33–42.